The RecA-directed recombination pathway of natural transformation initiates at chromosomal replication forks in the pneumococcus

Calum H G Johnston, Rachel Hope, Anne-Lise Soulet, Marie Dewailly, David de Lemos, Patrice Polard

PNAS RESEARCH ARTICLE | MICROBIOLOGY

The RecA-directed recombination pathway of natural transformation initiates at chromosomal replication forks in the pneumococcus

Calum H. G. Johnston[a,b], Rachel Hope[a,b,c], Anne-Lise Soulet[a,b], Marie Dewailly[a,b], David De Lemos[a,b], and Patrice Polard[a,b,1]

Edited by Alan Grossman, Massachusetts Institute of Technology, Cambridge, MA; received August 12, 2022; accepted December 9, 2022

Homologous recombination (HR) is a crucial mechanism of DNA strand exchange that promotes genetic repair and diversity in all kingdoms of life. Bacterial HR is driven by the universal recombinase RecA, assisted in the early steps by dedicated mediators that promote its polymerization on single-stranded DNA (ssDNA). In bacteria, natural transformation is a prominent HR-driven mechanism of horizontal gene transfer specifically dependent on the conserved DprA recombination mediator. Transformation involves internalization of exogenous DNA as ssDNA, followed by its integration into the chromosome by RecA-directed HR. How DprA-mediated RecA filamentation on transforming ssDNA is spatiotemporally coordinated with other cellular processes remains unknown. Here, we tracked the localization of fluorescent fusions to DprA and RecA in *Streptococcus pneumoniae* and revealed that both accumulate in an interdependent manner with internalized ssDNA at replication forks. In addition, dynamic RecA filaments were observed emanating from replication forks, even with heterologous transforming DNA, which probably represent chromosomal homology search. In conclusion, this unveiled interaction between HR transformation and replication machineries highlights an unprecedented role for replisomes as landing pads for chromosomal access of tDNA, which would define a pivotal early HR step for its chromosomal integration.

natural transformation | homologous DNA recombination | DNA replication | RecA | DprA

Homologous recombination (HR) is a universal DNA strand exchange mechanism, which is vital to genome biology via its implication in specific pathways of DNA repair and genetic diversification (1–4). The widely conserved recombinases of the RecA/Rad51 family are core HR effectors that form dynamic nucleofilaments to promote exchange between complementary DNA sequences (5). These reactions are controlled and assisted by specific effectors, which define different HR pathways across all kingdoms of life. Any dysfunction in these HR assistants can alter cell development, threaten the integrity or adaptive capacity of the genome, and endanger cell survival (1, 6, 7).

Natural transformation is a programmed HR-directed horizontal gene transfer mechanism that is widespread in bacteria and promotes the shuffling of chromosomally encoded genetic information (8). As such, transformation facilitates adaptive responses to stresses, including the acquisition of new genetic traits such as antibiotic resistance and vaccine escape (8–10), as well as limiting the genetic drift of species by curing genomes of mobile genetic elements (11–14).

Transformation is a multistep DNA processing mechanism directed by proteins encoded by the recipient cell (Fig. 1*A*). Most of these are expressed during a distinct physiological state, defined as competence, which is triggered and regulated in different ways depending on the species (8). Transformation proteins first direct the uptake of exogenous double-stranded DNA (dsDNA) through the cell envelope to the periplasmic space (15–18); next, they couple the transport of a linear single-stranded DNA (ssDNA) strand across the cell membrane with degradation of its complementary strand (16, 19–22); internalized ssDNA is then integrated into the genome by RecA-directed HR at homology sites. A key conserved early effector of the HR pathway of transformation is the ssDNA-binding protein DprA, which specifically interacts with RecA to mediate its loading onto ssDNA (23–25). Next, as in all HR pathways, RecA polymerizes on the ssDNA to form a nucleofilament, referred to as the presynaptic filament, and promotes homology search in chromosomal DNA and pairing with a complementary DNA strand to generate a three-stranded DNA molecule, defined as the HR heteroduplex, synapse, or D-loop. Next, a helicase is involved in extending ssDNA incorporation in the genome from the D-loop, which differs from one species to another. In firmicutes, this HR motor is RadA, a protein which also acts with RecA in pathways of DNA repair (26, 27). In contrast, a dedicated helicase ComM performs this DNA branch migration on the transformation D-loop in all other

Significance

Natural transformation is a central horizontal gene transfer (HGT) mechanism of genome plasticity in bacteria. It relies on the capture and transport of exogenous DNA across the cell envelope, followed by its recombination at homologous chromosomal DNA sites. We investigated in *Streptococcus pneumoniae* the spatiotemporal choreography of the early recombination steps of transformation, coordinated by the conserved DprA protein and the general RecA recombinase on transforming DNA (tDNA). DprA and RecA accumulate in a tDNA-dependent manner at chromosomal replication forks, in a minute timescale. RecA assembles dynamic filaments at those sites, as at DNA-damaged sites during their recombinational repair. Thus, RecA-directed tDNA homology search on the chromosome appears to initiate and proceed from the replication forks in *S. pneumoniae.*

Author contributions: C.H.G.J. and P.P. designed research; C.H.G.J., R.H., A.-L.S., and M.D. performed research; C.H.G.J., D.D.L., and P.P. contributed new reagents/analytic tools; C.H.G.J., A.-L.S., D.D.L., and P.P. analyzed data; C.H.G.J. and P.P. coordinated the research; and C.H.G.J. and P.P. wrote the paper.

The authors declare no competing interest.

This article is a PNAS Direct Submission.

[1]To whom correspondence may be addressed. Email: patrice.polard@univ-tlse3.fr.

This article contains supporting information online at https://www.pnas.org/lookup/suppl/doi:10.1073/pnas.2213867120/-/DCSupplemental.

Published February 16, 2023.

bacterial species (28). The final reactions of transformation, including covalent linkage and integration of the paired ssDNA molecule with the recipient chromosomal dsDNA, remain uncharacterized. Ultimately, a replication cycle generates a wild-type and a transformed chromosome, each segregated into a daughter cell.

Our current understanding of the transformation mechanism results from studies conducted in a dozen distinct species, including the historical models *Bacillus subtilis* and *Streptococcus pneumoniae* (the pneumococcus), as well as many other human pathogens such as *Haemophilus influenzae, V. cholerae,* and *Helicobacter pylori* (for reviews, see refs. 8, and 29). These studies highlighted important general features of transformation, including the remarkable speed at which transforming DNA (tDNA) is captured, internalized, and integrated into the chromosome. This was shown to occur in a minute time frame in *S. pneumoniae* and *V. cholerae* (30, 31). How the HR system of transformation achieves such efficiency is unexplained. Pioneering studies in *B. subtilis* reported the gradual and stable accumulation of GFP fusions to transformation proteins involved in tDNA uptake and ssDNA transport, as well as RecA, at one pole of competent cells independent of tDNA addition (32, 33). In the presence of tDNA, polar RecA evolved into filaments proposed to represent presynaptic filaments formed during the polar entry of ssDNA, which next scan chromosomal DNA for homology (33, 34).

Here, we investigated DprA and RecA localization dynamics during transformation in *S. pneumoniae*. In stark contrast to *B. subtilis*, in which competence occurs in nonreplicating cells and lasts for several hours, pneumococcal competence occurs during

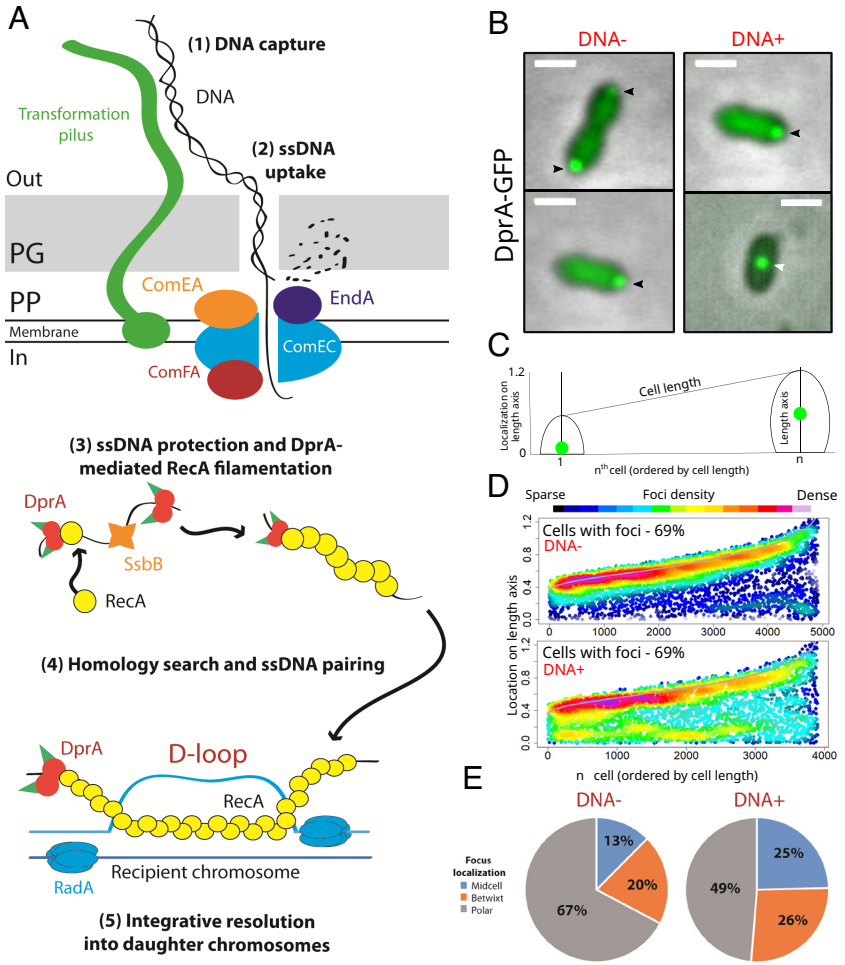

Fig. 1. DprA and HR during transformation. (*A*) Schematic representation of the steps involved in pneumococcal transformation 1) DNA capture. DNA is captured by a long transformation pilus, formed from the ComG proteins, and transferred to the DNA receptor ComEA. 2) ssDNA uptake. ComEA transfers the DNA to EndA, which degrades one strand of DNA, with the remaining single strand pulled through the ComEC transformation pore by the ComFA ATPase. 3) ssDNA protection and DprA-mediated RecA filamentation. Once internalized, ssDNA interacts with SsbB and the RMP DprA, which loads RecA onto the DNA. Polymerization of RecA along the ssDNA generates the early HR intermediate known as the presynaptic filament. 4) Homology search and ssDNA pairing. The presynaptic filament interacts with the chromosome in an unknown manner, and RecA promotes homology search. Once homology is found, the homologous strand of the recipient chromosome is displaced, and RecA facilitates pairing between the transforming ssDNA and the complementary strand, forming the so-called displacement loop (D-loop). D-loop extension is facilitated by the helicase RadA which unwinds the recipient chromosome on either side of the D-loop. 5) Integrative resolution into daughter chromosomes. The D-loop structure is resolved by the passage of the replication machinery, generating one transformed and one untransformed daughter chromosome. (*B*) Sample fluorescence microscopy images of R3728 strain (*comC0, dprA-gfp*) producing DprA-GFP 15 min after competence induction and 5 min after DNA addition (250 ng μL^{-1}). (Scale bars, 1 μm.) Black arrows, polar DprA-GFP foci; white arrows, midcell DprA-GFP foci. (*C*) Schematic representation of focus density maps with half-cells represented as vertical lines in ascending size order and localization of foci represented along the length axis of each half-cell. (*D*) Addition of transforming DNA significantly shifts ($P < 0.0001$) the localization profile of DprA-GFP foci toward midcell. Data represented as focus density maps plotted on the longitudinal axis of half-cells ordered by cell length. Each spot represents the localization of an individual focus, and spot colour represents focus density at a specific location on the half-cell. Cells with > 0 foci shown for each time point. In cells possessing > 1 foci, foci were represented adjacently on cells of the same length. DNA-: 5,739 cells and 4,920 foci analyzed; DNA+: 3,406 cells and 3,899 foci analyzed. (*E*) Localization of DprA-GFP foci along the longitudinal axis of a cell split into three categories on a half-cell of arbitrary length 1 where midcell is 0 and the pole is 1. Midcell, 0 to 0.3; betwixt, 0.3 to 0.7; polar, 0.7 to 1. DNA-, midcell, 13% ± 3; betwixt, 20 ± 4; polar, 67% ± 2. DNA+, midcell, 25% ± 3; betwixt, 26% ± 3; and polar, 49% ± 5. Values and SDs calculated from triplicate repeats.

the exponential phase of growth for a short period of about 30 min (35). In addition, tDNA is captured and enters competent *S. pneumoniae* cells not at the pole but at midcell (36, 37). Using fluorescent fusions of DprA and RecA, we tracked the early HR intermediates of transformation in actively transforming pneumococcal cells. Both proteins formed distinct foci at midcell in transforming cells, dependent on their physical interaction, showing that these nucleoprotein assemblies represent early HR intermediates of transformation. Furthermore, DprA and RecA foci were shown to localize to chromosomal replication forks. Importantly, RecA was observed to form short, dynamic filaments emanating from this replisomal accumulation point, possibly revealing homology search on the chromosome. These results represent an unprecedented link between the HR machinery of natural transformation and the chromosomal replication apparatus, shedding light on the mechanism of targeted homology search on the chromosome during pneumococcal transformation.

Results

DprA Accumulates at Midcell during Transformation in *S. pneumoniae*. To observe the early DprA-mediated HR steps of natural transformation in individual living competent pneumococcal cells, we tracked the localization of a fluorescent DprA-GFP fusion shown to be fully functional in transformation assays (38). Purified DprA-GFP was as efficient as DprA in assisting RecA-directed HR in an in vitro D-loop assay (*SI Appendix*, Fig. S1), validating the use of this fusion for analyzing DprA localization dynamics during transformation. We previously showed that DprA-GFP accumulated at a single cell pole in competent cells (38). This localization was related to an additional role for DprA in shut-off of pneumococcal competence. This negative feedback loop is independent of the ability of competent cells to uptake tDNA but dependent on a high cellular concentration of DprA (38, 39). Here, we analyzed DprA-GFP localization upon addition of tDNA to competent, transformable pneumococcal cells. Competence was induced by incubating cells with saturating levels (100 ng mL^{-1}) of synthetic competence-stimulating peptide (CSP) for 10 min (40), ensuring that all cells in the population were competent. Addition of saturating levels of tDNA (250 ng μL^{-1}) then ensured that all cells were engaging in transformation. The cells were visualized 5 min after tDNA addition and compared with cells without tDNA. DprA-GFP formed foci in competent cells, irrespective of the addition of tDNA (Fig. 1*B*). The frequency and cellular localization of DprA-GFP foci, presented as focus density maps ordered by cell length (Fig. 1*C*), showed that the addition of tDNA did not modify the frequency of foci in competent cells but significantly altered their localization ($P < 0.0001$, Fig. 1*D*), with an increase of midcell foci from 13 to 25 % (Fig. 1*E*). These results suggest that DprA-GFP interacts with internalized ssDNA to generate midcell foci.

We showed previously using a strain expressing *dprA* under the control of an IPTG-inducible P_{lac} promoter (CEP_{lac}-*dprA*) and lacking native *dprA* that reducing cellular levels of DprA in competent cells prevented competence shut-off from occurring whilst maintaining optimal transformation efficiency (39). Using a CEP_{lac}-*dprA-gfp* fusion, we also showed that in similar conditions (6 μM IPTG), no polar foci of DprA-GFP were observed (38). We took advantage of this strain and these conditions to visualize DprA-GFP during transformation as described above, with 48% of cells possessing DprA-GFP foci, mostly at midcell (Fig. 2 *A* and *B*). By contrast, only 7% of cells possessed foci in the absence of tDNA, in agreement with previous results (38). Most cells present DprA-GFP foci at midcell, while cells present foci at the ¼ and ¾ positions, future sites of midcell in daughter cells (Fig. 2*B*). To explore where these tDNA-dependent DprA-GFP foci localize along the lateral axis of the cells, data were represented as heatmaps split into six cell categories. tDNA-dependent DprA-GFP foci were present near the center of the longitudinal axis in all cell types (Fig. 2*C*). In nonconstricted cells, they were either side of the central axis, while in constricted cells, they appeared more central. Thus, DprA was found to accumulate at midcell in a tDNA-dependent manner. We next analyzed this localization at different time points after competence induction and tDNA addition. The results showed that the highest number of cells possessing tDNA-dependent DprA-GFP foci were observed 20 min after CSP addition and that the majority of cells with foci possess a single focus (*SI Appendix*, Fig. S2*A*). In addition, the localization profile of these foci remains similar over time (*SI Appendix*, Fig. S2*B*). Transforming cells with the same concentration of heterologous chromosomal DNA from *Escherichia coli* resulted in the formation of DprA-GFP foci at a similar frequency and localization (Fig. 2 *B* and *C*), showing that homology between tDNA and chromosomal DNA is not required for focus formation. We next examined how exogenous tDNA concentration influenced DprA-GFP focus formation. Results showed that a 1,000-fold reduction in tDNA concentration, starting from saturating conditions (250 ng μL^{-1}), reduced the frequency of cells exhibiting midcell DprA-GFP foci from 47 to 17 % (*SI Appendix*, Fig. S2*C*). This suggests that either more cells can take up DNA as the extracellular concentration increases, or cells can take up more DNA and thus more cells take up sufficient DNA to generate a DprA-GFP focus. In conclusion, pneumococcal DprA accumulates at two distinct locations in competent cells, correlating with its two roles in competence and transformation. First, as reported previously (38), the majority of DprA accumulates at one cell pole to mediate competence shut-off. Second, as observed here, a minority of DprA accumulates at midcell in a tDNA-dependent manner. This clustering of DprA at midcell appears therefore to be related to its role in transformation.

DprA Anchoring at Midcell Is Dependent on RecA. To gain further insights into the formation of tDNA-dependent DprA-GFP foci at midcell in competent cells, we reproduced these localization experiments in strains disrupted in three genes involved in different stages of the transformation process, i.e., *comEC*, *ssbB,* and *radA*. ComEC is proposed to form a channel in the cell membrane enabling ssDNA transfer into the cytoplasm (41). Only 2% of *comEC*$^-$ cells exhibited tDNA-dependent DprA-GFP foci, demonstrating that assembly of these foci depends on tDNA internalization (*SI Appendix*, Fig. S2*D*). Of note, it can be inferred from this result that DprA-GFP foci in competent cells grown without tDNA (Fig. 2) result from the internalization of DNA released in the medium from lysed cells. SsbB contributes to the protection and storage of internalized ssDNA to foster multiple chromosomal recombination events (42, 43), and RadA is a helicase that extends ssDNA integration at RecA-directed D-loop intermediates (26). Despite these key roles in transformation, neither was found to be involved in midcell DprA-GFP foci formation (*SI Appendix*, Fig. S3).

Next, we further explored DprA-GFP localization with two DprA point mutants, both severely impaired in transformation and differentially altered in DprA properties: $DprA^{AR}$, defective in dimerization and cooperative interaction with ssDNA and $DprA^{QNQ}$, disrupted in RecA interaction (24). Only 2% of transforming cells expressing the $DprA^{AR}$-GFP fusion from the ectopic P_{lac}-$dprA^{AR}$-*gfp* construct possessed foci (*SI Appendix*, Fig. S2*D*). In contrast, the $DprA^{QNQ}$-GFP fusion still formed central tDNA-dependent foci. However, these were observed in fewer cells than in

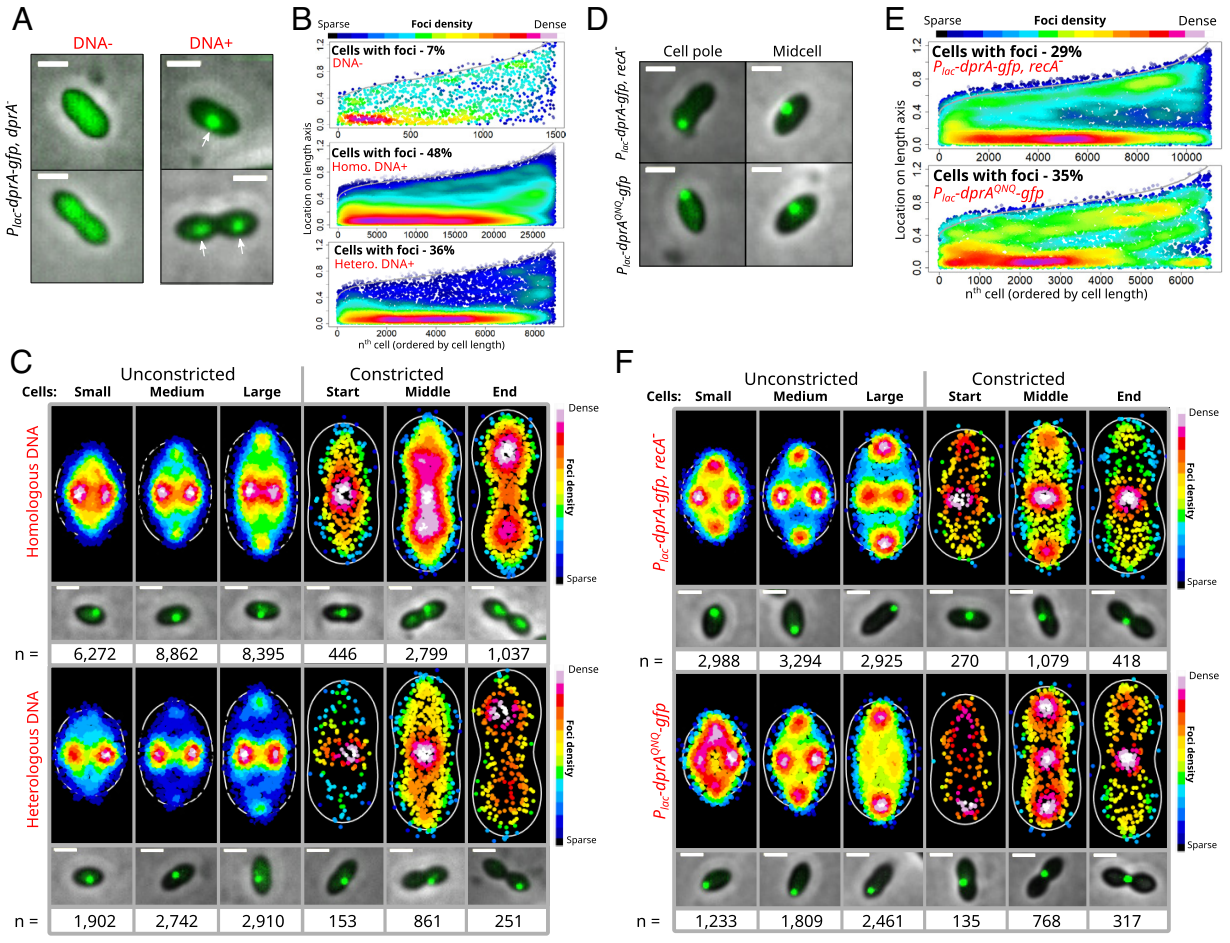

Fig. 2. When produced at low levels, DprA-GFP accumulates at midcell upon addition of transforming DNA, dependent on interaction with RecA. (*A*) Sample fluorescence microscopy images of R4262 strain (*comC0, CEP$_{lac}$-dprA-gfp, dprA::spc*) grown in 6 μM IPTG to produce ~300 DprA-GFP dimers, 15 min after competence induction and 5 min after DNA addition (250 ng μL^{-1}). (Scale bars, 1 μm.) White arrows, midcell DprA-GFP foci. (*B*) Low-level DprA-GFP accumulates at midcell upon addition of transforming DNA. Representations as focus density maps as described in Fig. 1*C*. DNA-: 21,055 cells and 1,512 foci analyzed; homologous DNA: 54,058 cells and 27,811 foci analyzed; and heterologous DNA: 23,962 cells and 8,819 foci analyzed. (*C*) Foci localization on density heat maps with cells split into six cell cycle categories by size and constriction status (see *Materials and Methods*). White lines represent the average cell contour of the sample set and each spot represents an individual focus, with colour representing density. Microscopy images represent sample images of each cell category showing preferential focus localization. (Scale bars, 1 μm.) Homologous transforming DNA: small cells, 17,888 cells and 6,272 foci analyzed; medium cells, 16,744 cells and 8,862 foci analyzed; large cells, 13,659 cells and 8,395 foci analyzed; cons. start cells, 880 cells and 446 foci analyzed; cons. middle cells, 3,824 cells and 2,799 foci analyzed; and cons. end cells, 1,063 cells and 1,037 foci analyzed. Heterologous transforming DNA: small cells, 7,557 cells and 1,902 foci analyzed; medium cells, 7,562 cells and 2,742 foci analyzed; large cells, 6,318 cells and 2,910 foci analyzed; cons. start cells, 377 cells and 153 foci analyzed; cons. middle cells, 1,708 cells and 861 foci analyzed; and cons. end cells, 440 cells and 251 foci analyzed. (*D*) Sample fluorescence microscopy images of low-level DprA-GFP foci within cells of R4415 (*comC0, CEP$_{lac}$-dprA^{QNQ}-gfp, dprA::spc*) and R4429 (*comC0, CEP$_{lac}$-dprA-gfp, dprA::spc, recA::cat)* strains 15 min after competence induction and 5 min after DNA addition (250 ng μL^{-1}). (Scale bars, 1 μm.) (*E*) Low-level DprA-GFP foci change localization profile in the absence of *recA* of in a *dprA^{QNQ}-gfp* mutant which cannot interact with RecA. Representations focus density maps as described in Fig. 1*C*. R4415, 7,912 cells and 6,723 foci analyzed and R4429, 35,318 cells and 10,974 foci analyzed. (*F*) Foci localization on density heat maps as described in *panel C* for R4415 (*comC0, CEP$_{lac}$-dprA^{QNQ}-gfp, dprA::spc*) and R4429 (*comC0, CEP$_{lac}$-dprA-gfp, dprA::spc, recA::cat*) strains. Data used as in panel *E*. Microscopy images represent sample images of each cell category showing preferential focus localization. (Scale bars, 1 μm.) R4415: small cells, 2,729 cells and 1,233 foci analyzed; medium cells, 2,180 cells and 1,809 foci analyzed; large cells, 2,132 cells and 2,461 foci analyzed; cons. start cells, 131 cells and 135 foci analyzed; cons. middle cells, 559 cells and 768 foci analyzed; and cons. end cells, 181 cells and 317 foci analyzed. R4429: small cells, 14,338 cells and 2,988 foci analyzed; medium cells, 9,534 cells and 3,294 foci analyzed; large cells, 7,508 cells and 2,925 foci analyzed; cons. start cells, 727 cells and 270 foci analyzed; cons. middle cells, 2,534 cells and 1,079 foci analyzed; and cons. end cells, 740 cells and 418 foci analyzed.

an isogenic wild-type DprA-GFP fusion and their localization on the longitudinal axis was significantly different, with a more even spread of central and polar foci observed ($P > 0.0001$, Fig. 2 *D* and *E* and *SI Appendix*, Fig. S2*E*). However, when the data were represented as heatmaps, with cells split into six size categories, the position of centrally localized foci on the lateral axis was markedly different. DprA^{QNQ}-GFP accumulated at the extremities of the lateral cellular axis in small and medium sized cells and at cell poles in large cells or at the constriction site and/or at the pole in constricted cells (*SI Appendix*, Fig. S2*F*). Thus, the localization patterns of DprA-GFP and DprA^{QNQ}-GFP foci markedly differ: The latter preferentially form foci in cellular areas not favored by the former, including the cell pole and lateral extremities. This result strongly suggested that DprA interaction with RecA is key for the tDNA-dependent midcell accumulation of DprA-GFP. To confirm this, we repeated the experiment with the low-level DprA-GFP fusion in a *recA*$^{-}$ mutant, and the results were significantly different from wildtype ($P < 0.0001$) and reminiscent of those observed with DprA^{QNQ}-GFP (Fig. 2 *D*–*F* and *SI Appendix*, Fig. S2*E*). These results show that the accumulation of DprA-GFP at midcell depends on DprA interaction with RecA and tDNA. Thus, this midcell accumulation point appears to attract a trio of cross-interacting partners, i.e., DprA, RecA, and tDNA. Importantly, when RecA or DprA is absent, most internalized ssDNA molecules are rapidly degraded (30). Transforming cells of a *recA comEC* double mutant showed almost no DprA-GFP foci (*SI Appendix*, Fig. S2 *F* and *G*). This suggested that sufficient internalized ssDNA remains protected by DprA within *recA*$^{-}$ competent cells to enable DprA-GFP foci

formation. Together, these results show that RecA drives midcell localization of DprA-GFP foci.

RecA Accumulates at Midcell during Transformation. The dependency on RecA for the midcell localization of DprA-GFP foci during transformation led us to analyze RecA localization in competent cells. However, a *recA-mturquoise* fluorescent gene fusion generated at the native *recA* locus, despite being produced at wild-type levels, was only partially functional in directing transformation and recombination repair of chromosomal damages (*SI Appendix,* Fig. S4). In addition, this RecA-mTurquoise fusion accumulated at the cell poles during competence, and DprA-YFP accumulated at this cell location when *dprA-yfp* was expressed at low concentrations in cells possessing RecA-mTurquoise (*SI Appendix,* Fig. S5). In an attempt to visualize RecA localization under fully functional recombination conditions, we placed the *recA-mturquoise* construct under the control of IPTG-inducible P_{lac} promoter at the ectopic chromosomal CEP locus, allowing the production of a mixture of RecA and RecA-mTurquoise proteins in the cells, a strategy successfully used in various species (44–46). This merodiploid strain, referred to as *recA*/*recA-mturquoise*, was equally as proficient in transformation and genome maintenance as the wild-type strain (*SI Appendix,* Fig. S4), showing that the localization of RecA-mTurquoise could be taken to represent a functionally relevant localization in this genetic context. In this context, we found that RecA-mTurquoise accumulates into fluorescent foci at midcell in competent cells, dependent on tDNA, displaying the same foci localization profile as cells expressing low-level DprA-GFP under the same conditions (Fig. 3 *A*–*C*). This result strongly suggests that midcell foci represented a functional cellular localization for RecA and DprA during transformation. Indeed, the formation of RecA-mTurquoise midcell foci was found to be dependent on tDNA and DprA (Fig. 3*D*). In addition, the formation of foci was not observed in $dprA^{QNQ}$ cells, where RecA–DprA interaction is abrogated (24) (Fig. 3*D*). Repeating this experiment in an IPTG gradient revealed that reducing the cellular levels of RecA-mTurquoise reduced the number of transforming competent cells with foci (*SI Appendix,* Fig. S2*A*). In addition, reducing the length of tDNA fragment reduced the number of cells presenting RecA-mTurquoise foci (Fig. 3*E*). This interdependency between DprA and RecA for their midcell accumulation highlights the role of DprA in HR as a mediator of RecA loading on ssDNA at this precise cell location. Finally, we also attempted to directly visualize internalized ssDNA by fluorescent labeling as previously described in *B. subtilis* (47). However, we were unable to conclusively visualize fluorescently labeled tDNA internalized in competent pneumococcal cells, which was essentially found randomly retained into multiple patches on the cell surface or in the periplasmic space as reported recently with *B. subtilis* (19) (*SI Appendix, Results* and Fig. S7). Together, these localization studies of DprA and RecA in transforming competent cells revealed their interdependent assembly into foci at midcell, which are functionally linked to their concerted role in directing the early HR steps of transformation.

DprA and RecA Colocalize with Chromosomal DNA Replication Forks in Transforming Cells. The localization of midcell tDNA-dependent DprA-GFP and RecA-mTurquoise foci was very similar to the localization of the replication forks of the chromosome tracked by using fusions to proteins of the replisome (48). To explore whether these foci colocalized with chromosomal replication forks, a strain was generated allowing controlled, ectopic expression of both the replisomal DnaX protein fused to YFP (CEP_M-*yfp-dnaX*; induced by maltose) and DprA-mTurquoise ($CEPII_{lac}$-*dprA-mturquoise*; induced by IPTG). In this strain, *yfp-dnaX* was expressed along with native *dnaX*, and YFP-DnaX displayed a localization profile resembling that of a previously published, functional DnaX-GFP fusion (48), suggesting a functionally relevant localization of DnaX in this genetic context. First, 81% (±3, 9%) of non-competent cells possessed at least one YFP-DnaX focus, while this was slightly reduced to 73 % (±1, 6%) in competent cells 20 min after CSP addition (*SI Appendix,* Fig. S8 *A*–*C*), showing that most replisomes remain intact in competent pneumococcal cells. Next, repeating the transformation experiment in this strain revealed that the cellular distribution of foci was almost identical for both fusions (Fig. 4 *A* and *B*). Then, 83,4 % of DprA-mTurquoise foci colocalized with YFP-DnaX foci (Fig. 4*C*), irrespective of the cell cycle stage of the cell. The replisome protein DnaX moves dynamically around midcell (48). Time-lapse microscopy of both DprA-mTurquoise and YFP-DnaX in competent, transforming cells showed that their midcell foci exhibited the same dynamics (Movie S1 and Fig. 4*D*). Foci dynamics were also analyzed for midcell foci generated by a fraction of transforming cells possessing DprA-mTurquoise expressed at native levels, with similar dynamics of midcell colocalization with YFP-DnaX observed (Fig. 4*E*). In all, this demonstrated that early DprA-mediated transformation HR intermediates navigate with replisomes. To strengthen this conclusion, ChIP-PCR experiments were carried out to explore whether YFP-DnaX was in close proximity to tDNA in transforming cells. First, results showed that a heterologous tDNA PCR fragment was copurified with DprA-GFP and DprA-YFP at 10-fold higher levels than with the $DprA^{AR}$-GFP dimerization mutant or the unfused GFP used as a negative control (Fig. 4*F*). Second, this tDNA was copurified with YFP-DnaX at a similar level to DprA-GFP (Fig. 4*G*), suggesting close proximity between early DprA-mediated HR intermediates and chromosomal replication forks during transformation. We also used a NanoBit assay (49–51) to explore the proximity of DprA, engaged in transformation, with the replisome. This system employs a luciferase separated into a large bit (LgBit) and a small bit (SmBit). Fusion of each part to different proteins that interact or are in close proximity in cells can restore luciferase activity and produce light in the presence of a furimazine-based substrate (51). A strain producing DprA-LgBit and an ectopic DprA-SmBit was used as a positive control and competent cells demonstrated strong luminescence irrespective of tDNA addition, due to dimerization of DprA (Fig. 4*H*). The LgBit tag was fused to the Cter of DprA, $DprA^{AR}$, or $DprA^{QNQ}$, and the SmBit was fused to the Cter of DnaX. Addition of tDNA to competent cells increased luminescence in cells coexpressing DnaX-SmBit and DprA-LgBit but not DnaX-SmBit, $DprA^{AR}$-LgBit, or $DprA^{QNQ}$-LgBit (Fig. 4*H*). This result further demonstrated a close proximity between the replisome and DprA, dependent on tDNA. Then, to formally demonstrate that RecA is also targeted to chromosomal replication forks during transformation, we analyzed RecA-mTurquoise localization in *recA*/*recA-mturquoise* competent cells coexpressing YFP-DnaX. As expected, RecA-mTurquoise foci were found to strongly colocalize with YFP-DnaX at midcell in transforming cells (Fig. 5 *A*–*C*).

RecA Forms Dynamic tDNA-Dependent Filaments at Chromosomal Replication Forks. In experiments investigating the localization of RecA-mTurquoise in the *recA*/*recA-mturquoise* strain, we observed filamentous fluorescent structures in a minority of non-competent cells (8%). These long polymers (0,82 µm ± 0,28 µm) appear similar to RecA filaments reported as HR filaments involved in recombinational repair of double-strand breaks (DSB) in other bacteria (44–46). Similarly, exposure of non-competent pneumococcal cells to DNA damaging agent norfloxacin increased the number of cells presenting long, dynamic RecA polymers, averaging 0,84 µm (± 0,31 µm) in length, from 8%

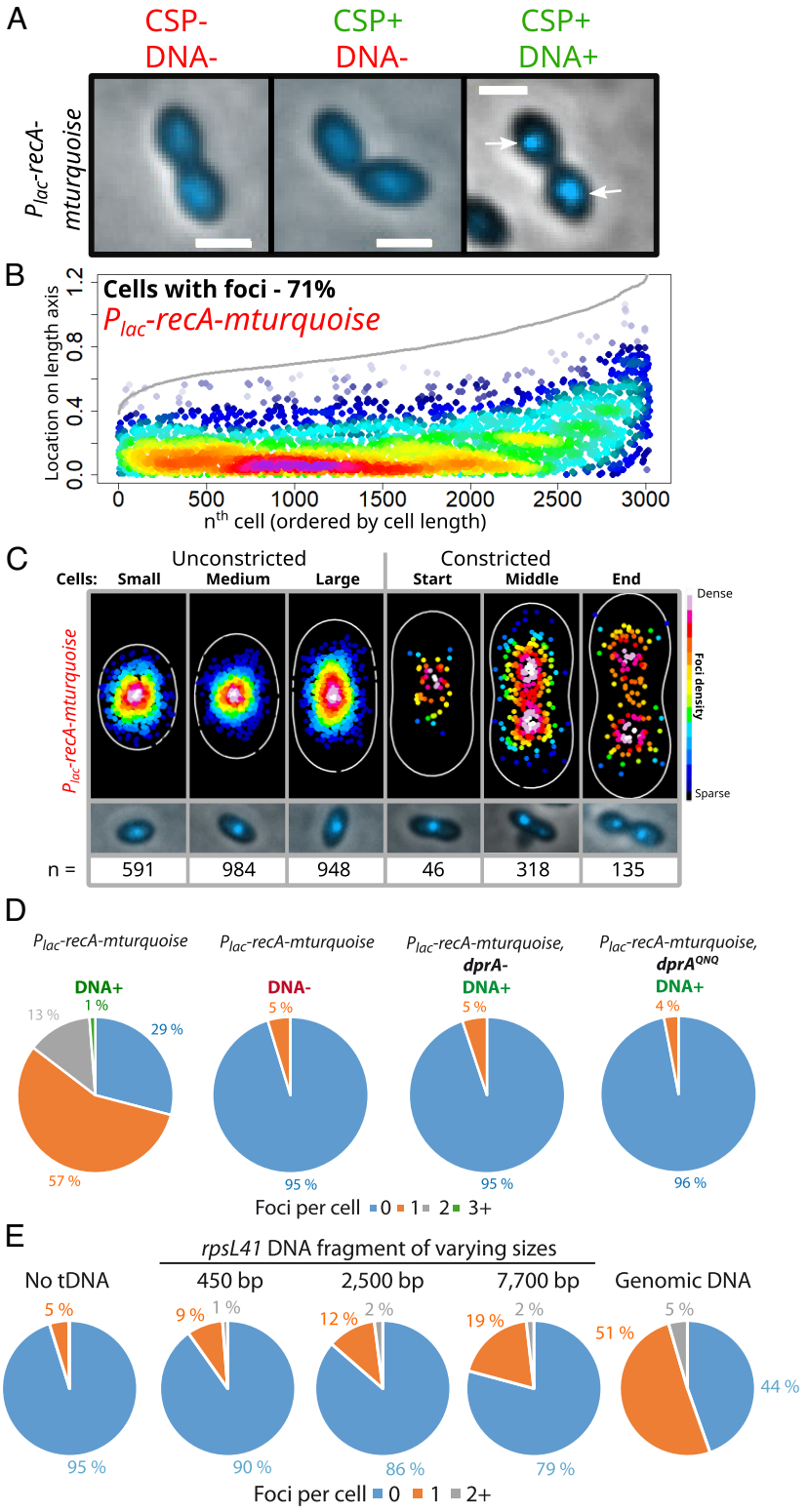

Fig. 3. Mixed filaments of RecA/RecA-mTurquoise accumulate at midcell during competence, dependent on tDNA. (*A*) Sample microscopy images of RecA/RecA-mTurquoise mixed filaments in non-competent cells and competent cells in the presence or absence of homologous tDNA. Images taken 15 min after competence induction. Strain used, R4848 (*comC0, P_{lac}-recA-mturquoise*). White arrows, midcell RecA-mTurquoise foci. (*B*) Mixed filaments of RecA/RecA-mTurquoise accumulate at midcell, reminiscent of DprA. Representations as focus density maps as described in Fig. 1*C*. *P_{lac}-recA-mturquoise*: 3,481 cells and 3,022 foci analyzed. (*C*) RecA/RecA-mTurquoise mixed filaments accumulate at midcell in transforming cells. Representations on density heat maps as described in Fig. 2*C*. Microscopy images represent sample images of each cell category showing preferential focus localization. Small cells, 923 cells and 591 foci analyzed; medium cells, 1,242 cells and 984 foci analyzed; large cells, 958 cells and 948 foci analyzed; cons. start cells, 45 cells and 46 foci analyzed; cons. middle cells, 229 cells and 318 foci analyzed; and cons. end cells, 84 cells and 135 foci analyzed. (*D*) Formation of RecA-mTurquoise foci expressed from *P_{lac}-recA-mturquoise* ectopic expression platform in merodiploid cells is dependent on tDNA and DprA. Strains used, *P_{lac}-recA-mturquoise*, R4848 (*comC0, CEP_{lac}-recA-mturquoise*) and *P_{lac}-recA-mturquoise, dprA*$^{-}$, R4851, (*comC0, CEP_{lac}-recA-mturquoise, dprA::spc*). DNA+, 0 foci, 29% ± 3; 1 focus, 57% ± 3; 2 foci, 13% ± 3; 3+ foci, 1% ± 2. DNA-, 0 foci, 95% ± 4; 1 focus, 5% ± 3. DNA+, *dprA-*, 0 foci, 95% ± 3; 1 focus, 5% ± 2. DNA+, *dprA^{QNQ}*, 0 foci, 96% ± 1; 1 focus, 4% ± 1. Values and SDs calculated from triplicate repeats. (*E*) Formation of RecA-mTurquoise foci expressed from *P_{lac}-recA-mturquoise* ectopic expression platform in merodiploid cells varies depending on the length of tDNA fragments used. Strain used, *P_{lac}-recA-mturquoise*, R4848 (*comC0, CEP_{lac}-recA-mturquoise*). No tDNA, 0 foci, 95% ± 1; 1 focus, 5% ± 1. 450 bp, 0 foci, 90% ± 1; 1 focus, 9% ± 1; 2+ foci, 1% ± 1. 2,500 bp, 0 foci, 86% ± 3; 1 focus, 12% ± 3, 2+ foci, 2% ± 1. 7,700 bp, 0 foci, 79% ± 2; 1 focus, 19% ± 2, 2+ foci, 2% ± 1. Genomic DNA, 0 foci, 44% ± 3; 1 focus, 51% ± 2, 2+ foci, 5% ± 2. Values and SDs calculated from triplicate repeats.

to 69.8% (Movies S2 and S3 and *SI Appendix,* Fig. S9). Notably, in transforming cells of this strain, we observed that 59% (± 5%) of RecA-mTurquoise foci colocalizing with replisomes exhibited dynamic filaments emanating from these foci (Fig. 5*D*). We used time-lapse microfluidics to track RecA-mTurquoise and YFP-DnaX localization in real time in transforming cells (52). Results showed rapid formation of RecA-mTurquoise foci in the vicinity of the replisome as little as 2 min after tDNA addition and subsequent dynamic extension of filaments (Fig. 5*E* and Movie S4). In contrast to the RecA filaments formed in cells exposed to norfloxacin, those that emanate from replication forks in transformed cells were short, extending on average 0.22 (± 0.05) μm either side of a replisome colocalization point. Similar short tDNA-dependent RecA filaments were observed with heterologous tDNA (genomic DNA from *E. coli*) (*SI Appendix,* Fig. S8 *D–F*) and, therefore, are not the result of pairing with a complementary sequence. Thus, these dynamic RecA polymers may represent presynaptic HR filaments assembled on tDNA and mediating homology search after having accessed the recipient chromosome via the replisome landing pad.

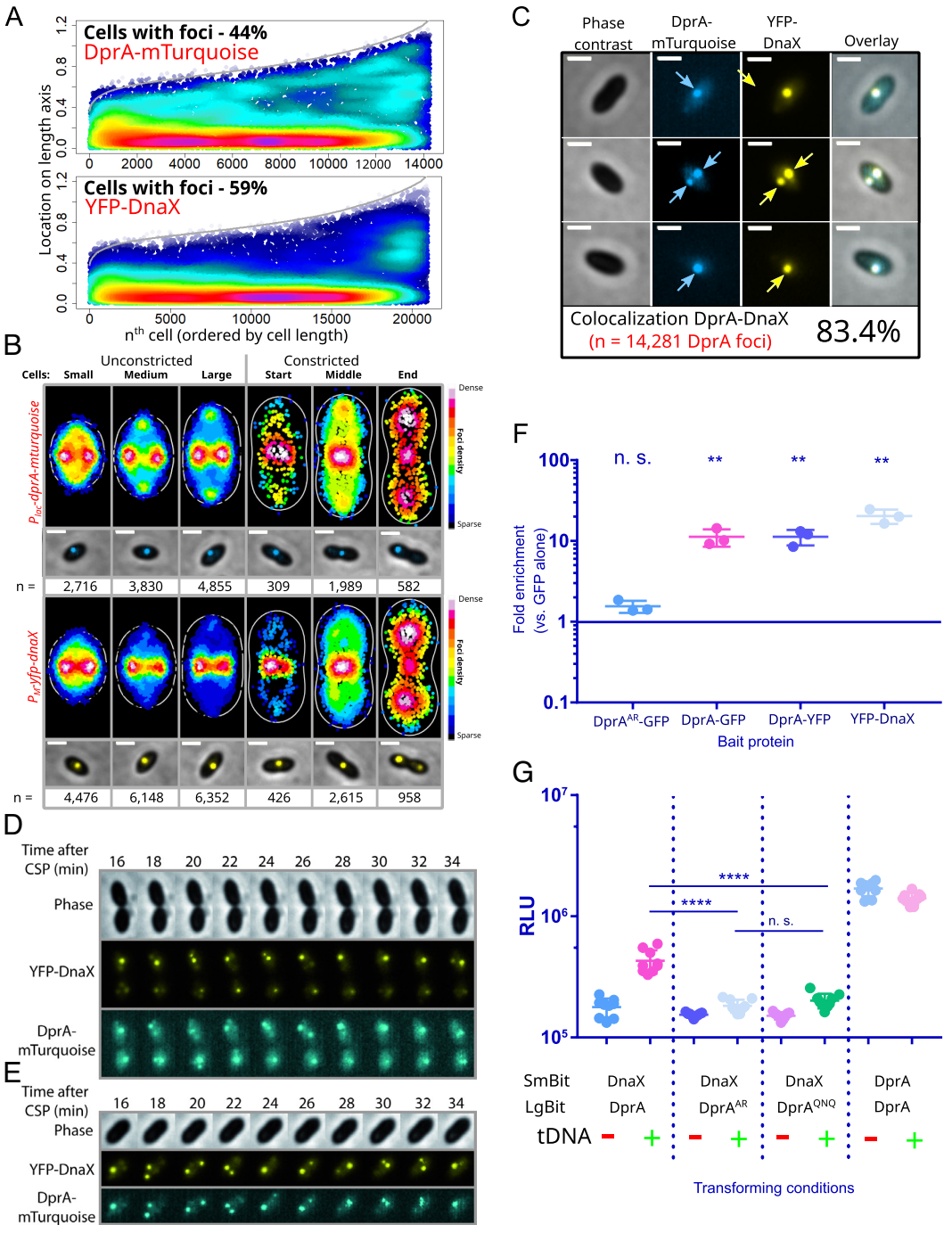

Fig. 4. HR intermediates of transformation interact with active chromosomal replication forks in competent cells. (*A*) Low-level DprA-mTurquoise foci display a localization profile similar to a YFP-DnaX fluorescent fusion of the replisome clamp loader expressed in the same R4631 cells (*comC0, CEP$_M$-yfp-dnaX, CEPIIP$_{lac}$-dprA-mTurquoise, dprA*$^-$). Representations as focus density maps as described in Fig. 1*C*. 29,942 cells analyzed possessing 14,281 DprA-mTurquoise foci and 20,975 YFP-DnaX foci analyzed. (*B*) DprA-mTurquoise and YFP-DnaX foci localization on density heat maps as described in Fig. 2*C* for R4631 strain. Data used as in panel *A*. Microscopy images represent sample images of each cell category showing preferential focus localization. Small cells, 9,979 cells, 2,716 DprA-mTurquoise, and 4,476 YFP-DnaX foci analyzed; medium cells, 8,517 cells, 3,830 DprA-mTurquoise, and 6,148 YFP-DnaX foci analyzed; large cells, 7,952 cells, 4,855 DprA-mTurquoise, and 6,352 YFP-DnaX foci analyzed; cons. start cells, 508 cells, 309 DprA-mTurquoise, and 426 YFP-DnaX foci analyzed; cons. middle cells, 2,390 cells, 1,989 DprA-mTurquoise, and 2,615 YFP-DnaX foci analyzed; cons. End cells, 596 cells, 582 DprA-mTurquoise, and 958 YFP-DnaX foci analyzed. (*C*) Sample microscopy images of R4631 strain expressing low level DprA-mTurquoise and YFP-DnaX and colocalization of DprA-mTurquoise with YFP-DnaX in these cells. Images taken 15 min after competence induction and 5 min after DNA addition (250 ng μL^{-1}). (Scale bars, 1 μm.) Phase contrast, phase contrast images of cells; overlay, overlay of all three other images. (*D*) DnaX and DprA produce similarly dynamic foci in competent, transforming cells. DprA-mTurquoise and YFP-DnaX observed during time-lapse microscopy of strain R4631 (*comC0, CEP$_M$-yfp-dnaX, CEPII-P$_{lac}$-dprA-mturquoise, dprA::spc*) starting 10 min after competence induction and 5 min after DNA addition. Images taken every 2 min. Phase, phase contrast images of cells. Overlay, a merge of the three other images. (Scale bars, 1 μm.) (*E*) DnaX and DprA colocalize at midcell in a fraction of cells when DprA is produced at wild-type levels. DprA-mTurquoise and YFP-DnaX observed during time-lapse microscopy of strain R5038 (*comC0, dprA-gfp, CEP$_M$-yfp-dnaX*) starting 10 min after competence induction and 5 min after DNA addition. Images taken every 2 min. Phase, phase contrast images of cells. Overlay, a merge of the three other images. (Scale bars, 1 μm.) (*F*) The replisome clamp loader DnaX interacts with transforming ssDNA in early HR intermediates, as shown by copurification of heterologous transforming ssDNA with YFP-DnaX at levels comparable to DprA-GFP and DprA-YFP in ChIP-PCR experiments. In contrast, DprA^{AR}-GFP copurified at levels comparable to the GFP alone negative control (with an enrichment value of 1, to which all other samples were normalized). Strains used: R2546, *comC0, CEP$_X$-gfp*; R3406, *comC0, CEP$_M$-yfp-dnaX*; R3728, *comC0, dprA-gfp*; R4046, *comC0, dprA^{AR}-gfp*; R4404, *comC0, dprA-yfp*. Asterisks represent significant difference between samples (** = P < 0.005, n. s. = not significant). DprA^{AR}-GFP, P = 0.52; DprA-GFP, P = 0.0029; DprA-YFP, P = 0.0019; YFP-DnaX, P = 0.0012. (*G*) Split-luciferase assay comparing cellular proximity of DnaX and DprA in presence or absence of tDNA. Luminescence signal increases when tDNA is added to competent cells containing *dprA-lgbit* and *dnaX-smbit* (R4856), indicating an increased proximity of these fusion proteins in the presence of tDNA. When *dprA-lgbit* is replaced by the dimerization mutant *dprA^{AR}-lgbit* (R4861) or the RecA interaction mutant *dprA^{QNQ}-lgbit* (R5043), the increase in luminescence upon addition of tDNA is attenuated. A strain containing *dprA-lgbit* and *P$_{lac}$-dprA-smbit* (R4858) was used as a positive control for interaction since DprA dimerises and shows high luminescence irrespective of tDNA addition. Each point represents an individual replicate, with nine replicates done for each condition. RLU, relative luminescence units. Asterisks represent significant difference between samples (**** = P < 0.0001). No significant difference observed between DNA- conditions with *dnaX-smbit* (P > 0.05).

Then, to test whether blocking DNA replication altered the capacity of DprA to mediate tDNA-dependent RecA filamentation at chromosomal replication forks, we reproduced these localization experiments in the presence of HpUra, a nucleotide analog that selectively inhibits the essential PolC DNA polymerase of the pneumococcal replisome (30, 53). We first analyzed RecA-mTurquoise

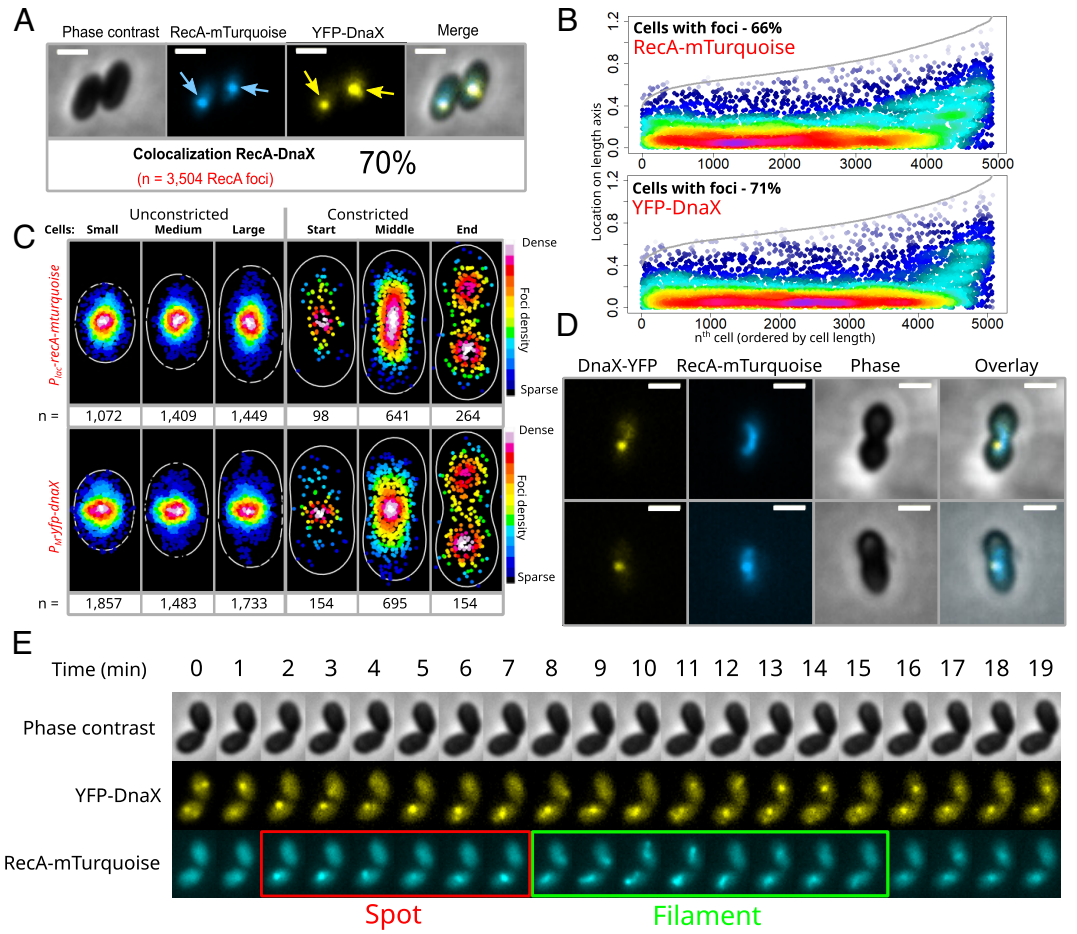

Fig. 5. RecA/RecA-mTurquoise filaments emanate from replication forks for homology search during transformation. (*A*) RecA-mTurquoise and YFP-DnaX colocalize in competent cells in the presence of tDNA. Strain used: R4840 (*comC0, ssbB::luc, CEP$_M$-yfp-dnaX, CEPIIP$_{loc}$-recA-mturquoise*). 5,866 cells, 4,923 RecA-mTurquoise foci, and 5,081 YFP-DnaX foci analyzed. (*B*) Focus density maps of RecA-mTurquoise and YFP-DnaX, as described in Fig. 1*C*. Strain, cell, and foci details as in panel *A*. (*C*) Heatmaps of RecA-mTurquoise and YFP-DnaX as described in Fig. 2*C*. Small cells, 1,730 cells, 1,072 RecA-mTurquoise, and 1,071 YFP-DnaX foci analyzed; medium cells, 1,766 cells, 1,409 RecA-mTurquoise, and 1,582 YFP-DnaX foci analyzed; large cells, 1,603 cells, 1,449 RecA-mTurquoise, and 1,582 YFP-DnaX foci analyzed; cons. Start cells, 93 cells, 88 RecA-mTurquoise, and 92 YFP-DnaX foci analyzed; cons. middle cells, 510 cells, 1,989 RecA-mTurquoise, and 614 YFP-DnaX foci analyzed; and cons. End cells, 165 cells, 264 RecA-mTurquoise, and 257 YFP-DnaX foci analyzed. (*D*) Microscopy images showing filaments of RecA-mTurquoise emanating from YFP-DnaX foci. (*E*) Time-lapse images of RecA-mTurquoise and YFP-DnaX in microfluidics experiment with time representing time after tDNA addition. Strain used as in panel *A*.

localization in non-competent *recA*/*recA-mturquoise* cells following the addition of the saturating amount of HpUra that fully blocks chromosomal DNA replication and cell growth (30, 54) (*SI Appendix,* Fig. S10*A*). We observed the formation of long RecA-mTurquoise filaments (0.94 μm ± 0.41 μm) 5 min after HpUra addition (*SI Appendix,* Fig. S10*B*), reproducing what was observed previously in *B. subtilis* (55). Importantly, these filaments were lost in cells lacking *recO*, showing that they depend on the RecFOR recombinase loading system (52, 53) (*SI Appendix,* Fig. S10*B*). We previously demonstrated that transformation is RecO independent (56). Thus, we analyzed RecA-mTurquoise and YFP-DnaX localizations in *recO*$^-$, *recA*/*recAmTurquoise*, and *yfp-dnaX* competent cells, to prevent the formation of HpUra-dependent and RecO-mediated RecA-mTurquoise filaments. Cells were exposed to HpUra for 5 min, then CSP was added to induce competence, and tDNA was added 10 min later. Cells were visualized after a further 5-min incubation to allow tDNA internalization. Results showed that first, YFP-DnaX still accumulated into midcell foci even after PolC-directed replication was blocked, showing that replisomes remained intact, although stalled (*SI Appendix,* Fig. S10 *C–F*). In transforming cells with stalled replisomes, RecA still accumulated into midcell foci, which strongly colocalized with DnaX-YFP (*SI Appendix,* Fig. S10 *C–F*), with RecA-mTurquoise filamentation emanating from replisome colocalization points also observed (*SI Appendix,* Fig. S10*G*). In conclusion, these results show that active replication is not required for RecA access to chromosomal forks during transformation and that RecO is not involved in tDNA-dependent RecA filamentation emanating from that precise chromosomal location.

Discussion

In this study, we reveal that the dedicated DprA-mediated and RecA-directed HR pathway of natural genetic transformation is spatiotemporally orchestrated at chromosomal replication forks in *S. pneumoniae* (Fig. 6*A*). First, by using genetic contexts where GFP fusions display functionally relevant localizations, we demonstrate that both DprA and RecA accumulate at midcell and colocalize with the replisome protein DnaX in a tDNA-dependent manner. These colocalizations are observed in ∼70 % of a competent, transforming population, roughly equivalent to the number of cells undergoing chromosomal replication at a given time in these growth conditions (Figs. 4 and 5). Second, we found that DnaX is in physical proximity to tDNA in transforming cells (Fig. 4*E*) and that tDNA addition promotes increased proximity between DnaX and DprA (Fig. 4*F*). Interdependent DprA and RecA accumulation at chromosomal replication forks following tDNA internalization

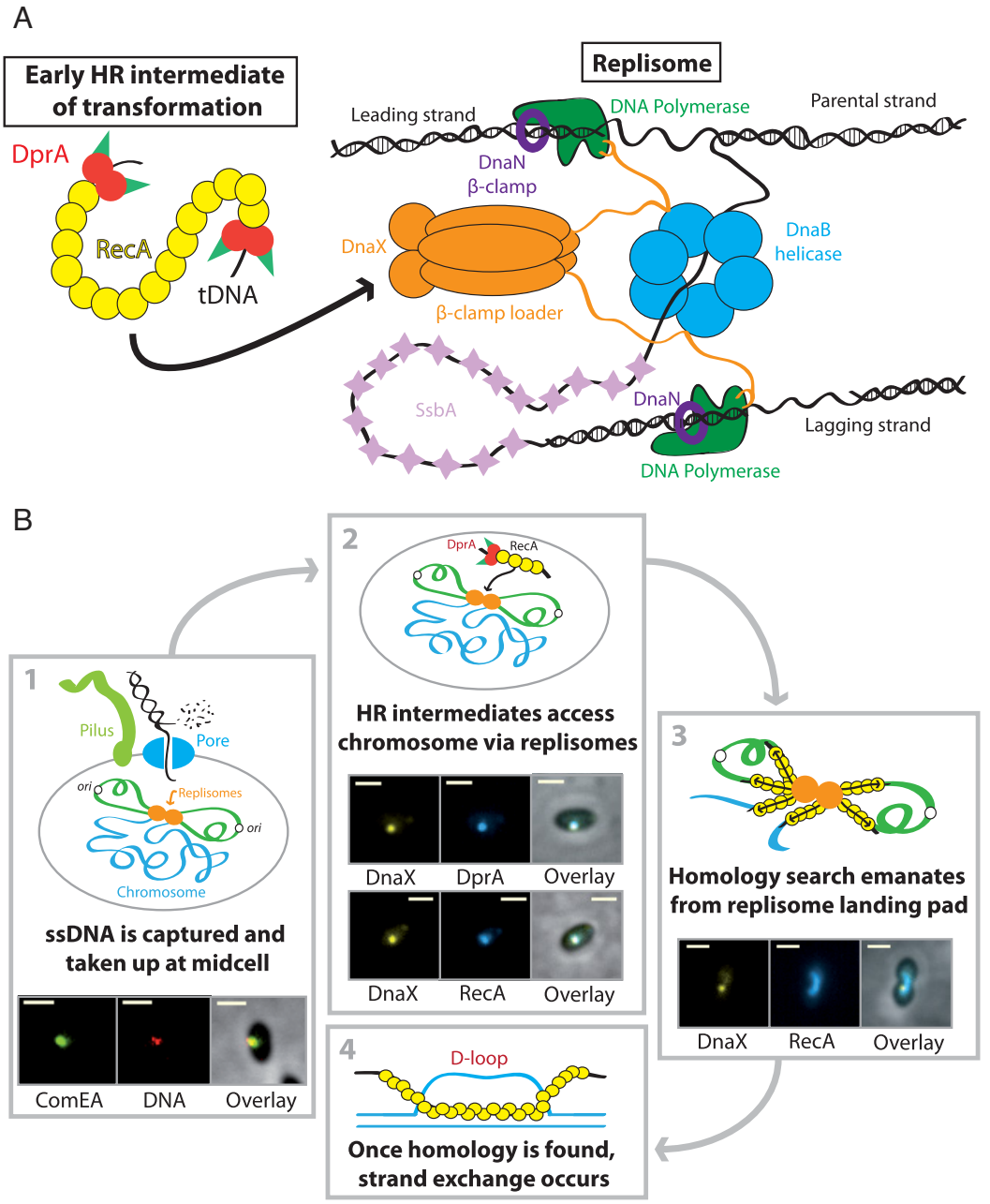

Fig. 6. Model of the interaction between transformation and replication complexes. (*A*) Tight connection between early HR intermediates of transformation, comprising of the transformation-dedicated RMP DprA, the recombinase RecA and transforming ssDNA, and active replisomes during pneumococcal transformation. Diagrammatic representation of the replisome architecture based on bacterial model from *E. coli*, adapted to the pneumococcus. (*B*) Model of the interaction between early HR intermediates of transformation and active replisomes, and how this may facilitate homology search during HR. 1—Transforming ssDNA is captured and internalized at midcell, providing a direct spatial link between incoming transformation nucleocomplexes and active replisomes also localized to midcell. Microscopy images taken from experiments carried out previously demonstrating colocalization of the DNA receptor ComEA and Cy3-labeled transforming DNA at midcell (37). (Scale bar 1 μm.) 2—Early HR intermediates comprising DprA, RecA, and tDNA access the chromosome via active replication forks. Microscopy images display the strong colocalization of both DprA and RecA with the replisome β-clamp loader DnaX, as shown in this study. (Scale bar 1 μm.) 3—RecA mediates homology search within the recipient chromosome, emanating from replication forks used as landing pads to access the chromosome. Microscopy images showing filamentation of RecA emanating from replication forks (shown via DnaX), as shown in this study. 4—Once homology is found, strand exchange occurs between the transforming ssDNA and the homologous strand of the recipient chromosome, generating a transformation D-loop which will be resolved by replication into one wildtype and one transformed chromosome.

matches the interplay between DprA, RecA, and ssDNA previously uncovered by combining biochemical and genetic analyses and proven to promote HR during transformation via the formation of the presynaptic HR filament (23, 24). Strong evidence supporting this conclusion is the formation of tDNA-dependent and DprA-mediated RecA filaments emanating from the replisome (Fig. 5 *D* and *E*). In addition, midcell DprA-GFP localization is not observed in a *comEC* mutant (*SI Appendix*, Fig. S2*D*), demonstrating the need for tDNA internalization to generate DprA and RecA foci by interaction with the internalized ssDNA template. Third, both DprA and RecA foci and RecA filaments are observed in a minute time frame in transforming cells. These kinetics are as rapid as that of tDNA integration into the pneumococcal chromosome tracked over time with the use of a short radiolabeled tDNA fragment homologous to a specific chromosomal locus (30). Fourth, both DprA and RecA foci and RecA filaments are formed at replication forks either with homologous or heterologous tDNA, in the same short time frame (Fig. 5 and *SI Appendix*, Fig. S8). Thus, we

suggest that the RecA filaments emanating from the replication forks in transforming pneumococcal cells may represent presynaptic HR intermediates engaged in the search of homology on the chromosome (Fig. 6*B*). Altogether, these findings link the HR machinery of transformation and the replisome for the first time in a naturally transformable bacterial species.

Dynamic RecA filaments formed at replication forks in transforming pneumococcal cells are similar to those of genome maintenance HR pathways visualized in single cells in several bacterial species and demonstrated to be presynaptic filaments actively searching for homology and promoting recombinational DNA repair (44–46). However, these RecA filaments exhibit marked differences compared to those of pneumococcal transformation reported here. Notably, the dynamic RecA filaments assembled at a single DSB on one copy of the neoreplicated chromosome of *E. coli* or *Caulobacter crescentus* extend across the cell length, which is proposed to correspond to the bidirectional search for the uncleaved homologous DNA on the second copy of the chromosome segregated to the opposite cell pole (44–46). We observed such long RecA filaments in growing pneumococcal cells suffering genome damages, including specific replication fork arrest caused by the HpUra PolC inhibitor as previously reported in *B. subtilis* (55) (*SI Appendix,* Fig. S10). In contrast, RecA filaments formed during pneumococcal transformation at replication forks are shorter (Fig. 5 *D* and *E*). One reason for this difference may be the length of the individual tDNA fragments entering the cell, evaluated to be in the range of 3 to 7 kb and gradually reduced over the competence window (43). Another marked difference between RecA filaments in HR pathways of pneumococcal transformation and genome maintenance is their assembly site in the cell. In the latter case, RecA filaments are formed on the chromosome at the site of DNA damage, in conjunction with the formation of ssDNA template. In contrast, in the case of pneumococcal transformation, ssDNA is formed and enters the cell at the cytoplasmic membrane through ComEC and must reach the replication fork where DprA-mediated RecA filamentation occurs. Therefore, ssDNA formation and presynaptic RecA filamentation appear to be spatially separated during transformation in the pneumococcus. Interestingly, however, tDNA capture and uptake were previously found to also occur at midcell in the pneumococcus (36, 37). Thus, transformation appears to proceed via a midcell channel coupling DNA capture and internalization with chromosome access and HR, which may underpin the speed at which transformation occurs in a minute time frame in the pneumococcus (30).

Previous analysis of RecA localization during transformation in *B. subtilis* depicted a different choreography than the one reported here for *S. pneumoniae*. Interestingly, transformation occurs in non-replicating *B. subtilis* cells, as shown by the lack of DnaX-GFP foci in competent cells (57) and GFP-RecA has been found to localize at one cell pole where the proteins directing tDNA capture and uptake accumulate (33). Upon transformation, GFP-RecA has been found to generate long filaments from the cell pole, proposed to represent homology search on chromosomal DNA (33). However, *B. subtilis* DprA was not found to follow the same choreography as it accumulates at midcell in transforming cells (34). These marked deviations in RecA filamentation dynamics during transformation between *S. pneumoniae* and *B. subtilis* run parallel to the difference in the timing of competence development between these two species. Pneumococcal competence is triggered in actively replicating cells in response to a large panel of stresses (35), including genome damage (54, 58, 59), and lasts for a short period of time of 30 min (60). In contrast, competence in *B. subtilis* occurs during nutrient starvation when cells stop replicating and lasts for several hours (8). Thus, transformable bacterial species have evolved distinct strategies to mediate HR-mediated chromosomal integration of tDNA, depending on how competence is integrated into their cell cycle. It will be interesting to explore how other transformable species integrate the early HR steps of transformation into their varied cell cycles. The anchoring of the presynaptic HR filaments of transformation to the chromosomal replication forks of *S. pneumoniae* not only provides them immediate access to chromosomal DNA for homology search but also to the potential actions of the large set of proteins acting at the forks, either directly in DNA replication or occasionally to repair the damaged forks (61–63). This toolbox of DNA effectors is ideally located to assist the whole HR process of transformation up to covalent linkage of tDNA to the chromosome, many steps of which remain uncharacterized. Of note, we demonstrate with HpUra-treated competent cells that the replication forks do not need to be active to act as molecular anchors for the early step of HR of transformation (*SI Appendix,* Fig. S10). This mirrors a previous study showing that HpUra-treated competent pneumococcal cells integrate tDNA as efficiently as non-treated cells (59). This indicates that RecA filaments spread over the genome for homology search, emanating from replication forks.

A major perspective of this study is to identify how early HR intermediates, composed of DprA and RecA bound to tDNA, are driven to the chromosomal replication forks. Many proteins are concentrated at these vital chromosomal sites, either essential or accessory to the DNA replication process (61–63). We show that RecA drives early HR intermediates to midcell (Fig. 2 *D*–*F*), opening up the possibility of an interaction between RecA and such a replication protein partner. One of these known accessory effectors is the RecO protein, which is known to mediate RecA loading on ssDNA gaps. However, we demonstrate that RecO is not needed for replisome access of early HR intermediates or RecA filamentation at replication forks (*SI Appendix,* Fig. S10). In addition, transformation HR effectors SsbB and RadA also played no role in this chromosome access mechanism (*SI Appendix,* Fig. S3).

In conclusion, this study revealed that early HR intermediates of pneumococcal transformation accumulate at chromosomal replication forks. By doing so, replication forks could provide a landing pad for presynaptic filaments of HR to access the recipient chromosome and carry out homology search, optimizing the speed and efficiency of transformation.

Materials and Methods

Bacterial Strains, Competence, and Transformation. The pneumococcal strains, primers, and plasmids used in this study can be found in *SI Appendix,* Table S1. Standard procedures for transformation and growth media were used (64). In this study, cells were prevented from spontaneously developing competence by deletion of the *comC* gene (*comC0*) (65). Precompetent cultures were prepared, and transformation was carried out as previously described (38). Antibiotic concentrations (μg mL^{-1}) used for the selection of *S. pneumoniae* transformants were chloramphenicol (Cm), 4.5; erythromycin, 0.05; kanamycin (Kan), 250; spectinomycin (Spc), 100; streptomycin (Sm), 200; and trimethoprim (Trim), 20. GraphPad Prism was used for statistical analyses. To compare two averages of triplicate repeats, an unpaired *t* test was used. To compare longitudinal distribution profiles of focus data, a non-parametric Kolmogorov–Smirnoff test was used. Detailed information regarding the construction of new plasmids and strains can be found in the *SI Appendix*. To compare protein expression profiles, Western blots were carried out as previously described (38). Primary polyclonal antibodies raised against RecA and SsbB were used at 1/10,000 dilution.

Fluorescence Microscopy and Image Analysis. To visualize cells by epifluorescence microscopy, pneumococcal precultures grown in a C + Y medium at 37 °C to an OD_{550} of 0.1 were induced with CSP (100 ng mL^{-1}). Cells were incubated for 10 min at 37 °C before the addition of transforming DNA. Transforming DNA

was either homologous (*S. pneumoniae* R1501 genomic DNA) or heterologous (*E. coli* genomic DNA) prepared using QIAGEN 500/g Genomic tips. The cells were then incubated at 37 °C for 5 min unless stated. After this incubation, 2 μL samples were spotted on a warmed microscope slide containing a slab of 1.2 % C + Y agarose as previously described (37) before imaging. To generate movies, images were taken of the same fields of vision at varying time points during incubation at 37 °C. Phase contrast and fluorescence microscopy were performed as previously described (66). Images were processed using the Nis-Elements AR software (Nikon). Images were analyzed using MicrobeJ, a plug-in of ImageJ (67). Data were analyzed in MicrobeJ or R and represented in two distinct ways. First, focus density maps were plotted on the longitudinal axis of half cells ordered by cell length. Each spot represents the localization of an individual focus, and the spot color represents focus density at a specific location on the half cell. Only cells with > 0 foci are shown. In cells possessing > 1 foci, foci were represented adjacently on cells of the same length. Second, the cells were separated into six categories based on the cell size and presence or absence of constriction, and heatmaps were generated for each category. The six cell categories were defined in MicrobeJ to reflect those determined previously for pneumococci (66). End of constriction (cons. end); septum = 1, circularity < 0.7; middle of constriction (cons. middle), septum = 1, 0.8 > circularity > 0.7; start of constriction (cons. start), all other cells with septum = 1; large cells, septum = 0, cell length > 1.4 μm, circularity < 0.9; medium cells, septum = 0, 1.4 μm > cell length > 1.2 μm, 0.94 > circularity < 0.9; and small cells, all other cells with septum = 0. The proportions of cells found in each category were consistent with those previously observed in these conditions (66), validating the parameters used to define the categories.

Chromatin Immunoprecipitation PCR (ChIP-PCR). Chromatin immunoprecipitation (ChIP) was done using magnetic GFP-Trap beads as per the manufacturer's instructions (Chromotek). Full details of the method used can be found in the *SI Appendix*. Relative quantification of qPCR data was performed with the $2^{-\Delta\Delta CT}$ method (68). Each PCR reaction, run in duplicate for each sample, was repeated at least two independent times. Data are represented as mean ± SEM calculated from triplicate repeats, with individual data points plotted.

Split-Luciferase Assay. Split luciferase assays were carried out as previously described (49–51), with modifications. Briefly, pneumococcal cells were grown in a C + Y medium (with 50 μM IPTG where required) at 37 °C until OD_{550} 0.1, and competence was induced by the addition of 100 ng mL^{-1} CSP. The cells were then incubated for 10 min at 37 °C before the addition of R1501 chromosomal DNA (250 ng μL^{-1}) where noted, followed by a further 5 min incubation at 37 °C. The cells were then washed in fresh C + Y medium and 1% NanoGlo substrate (Promega) was added and luminescence was measured 20 times every 1 min in a plate reader (VarioSkan luminometer, ThermoFisher). Data are represented as mean ± SEM calculated from nine independent repeats, with individual data points plotted.

Data, Materials, and Software Availability. All study data are included in the article and/or *SI Appendix*.

ACKNOWLEDGMENTS. We thank Isabelle Mortier-Barriere for the support with microfluidics experiments. We thank Jérome Rech for the support with microscopy and video assembly. We thank the LITC (Light Imaging Toulouse CBI) imaging platform of Toulouse TRI (Toulouse Réseau Imagerie) for their assistance in microscopy. This work was funded by the Centre National de la Recherche Scientifique, University Paul Sabatier, and the Agence Nationale de la Recherche (grants ANR-10-BLAN-1331 and ANR-17-CE13-0031).

Author affiliations: [a]Laboratoire de Microbiologie et Génétique Moléculaires, UMR5100, Centre de Biologie Intégrative, Centre Nationale de la Recherche Scientifique, 31062 Toulouse, France; [b]Université Paul Sabatier (Toulouse III), 31062 Toulouse, France; and [c]Department of Life Sciences, Imperial College, SW7 2AZ London, UK

1. B. Michel, D. Leach, Homologous recombination-enzymes and pathways. *EcoSal Plus* **5** (2012), 10.1128/ecosalplus.7.2.7.
2. W.-D. Heyer, K. T. Ehmsen, J. Liu, Regulation of homologous recombination in eukaryotes. *Annu. Rev. Genet.* **44**, 113–139 (2010).
3. L. Krejci, V. Altmannova, M. Spirek, X. Zhao, Homologous recombination and its regulation. *Nucleic Acids Res.* **40**, 5795–5818 (2012).
4. S. L. Lusetti, M. M. Cox, The bacterial RecA protein and the recombinational DNA repair of stalled replication forks. *Annu. Rev. Biochem.* **71**, 71–100 (2002).
5. J. C. Bell, S. C. Kowalczykowski, RecA: Regulation and mechanism of a molecular search engine. *Trends Biochem. Sci.* **41**, 491–507 (2016).
6. W.-D. Heyer, Regulation of recombination and genomic maintenance. *Cold Spring Harb. Perspect. Biol.* **7**, a016501 (2015).
7. N. Hunter, Meiotic recombination: The essence of heredity. *Cold Spring Harb. Perspect. Biol.* **7**, a016618 (2015).
8. C. Johnston, B. Martin, G. Fichant, P. Polard, J.-P. Claverys, Bacterial transformation: Distribution, shared mechanisms and divergent control. *Nat. Rev. Microbiol.* **12**, 181–196 (2014).
9. M. Blokesch, Natural competence for transformation. *Curr. Biol.* **26**, R1126–R1130 (2016).
10. A. B. Brueggemann, R. Pai, D. W. Crook, B. Beall, Vaccine escape recombinants emerge after pneumococcal vaccination in the United States. *PLoS Pathog.* **3**, e168 (2007).
11. N. J. Croucher *et al.*, Horizontal DNA transfer mechanisms of bacteria as weapons of intragenomic conflict. *PLoS Biol.* **14**, e1002394 (2016).
12. G. Carvalho, Bacterial transformation buffers environmental fluctuations through the reversible integration of mobile genetic elements.
13. O. H. Ambur, J. Engelstädter, P. J. Johnsen, E. L. Miller, D. E. Rozen, Steady at the wheel: Conservative sex and the benefits of bacterial transformation. *Philos Trans. R. Soc. Lond B Biol. Sci.* **371**, 20150528 (2016).
14. K. J. Apagyi, C. Fraser, N. J. Croucher, Transformation asymmetry and the evolution of the bacterial accessory genome. *Mol. Biol. Evol.* **35**, 575–581 (2018).
15. R. Laurenceau *et al.*, A type IV pilus mediates DNA binding during natural transformation in Streptococcus pneumoniae. *PLoS Pathog.* **9**, e1003473 (2013).
16. P. Seitz *et al.*, ComEA is essential for the transfer of external DNA into the periplasm in naturally transformable Vibrio cholerae cells. *PLoS Genet.* **10**, e1004066 (2014).
17. I. Chen, R. Provvedi, D. Dubnau, A macromolecular complex formed by a pilin-like protein in competent Bacillus subtilis. *J. Biol. Chem.* **281**, 21720–21727 (2006).
18. C. K. Ellison *et al.*, Retraction of DNA-bound type IV competence pili initiates DNA uptake during natural transformation in Vibrio cholerae. *Nat. Microbiol.* **3**, 773–780 (2018).
19. J. Hahn, M. DeSantis, D. Dubnau, Mechanisms of transforming DNA uptake to the periplasm of Bacillus subtilis. *mBio* **12**, e0106121 (2021).
20. A. Puyet, B. Greenberg, S. A. Lacks, Genetic and structural characterization of endA. A membrane-bound nuclease required for transformation of Streptococcus pneumoniae. *J. Mol. Biol.* **213**, 727–738 (1990).
21. G. S. Inamine, D. Dubnau, ComEA, a Bacillus subtilis integral membrane protein required for genetic transformation, is needed for both DNA binding and transport. *J. Bacteriol.* **177**, 3045–3051 (1995).
22. P. P. Damke *et al.*, Identification of the periplasmic DNA receptor for natural transformation of Helicobacter pylori. *Nat. Commun.* **10**, 5357 (2019).
23. I. Mortier-Barrière *et al.*, A key presynaptic role in transformation for a widespread bacterial protein: DprA conveys incoming ssDNA to RecA. *Cell* **130**, 824–836 (2007).
24. S. Quevillon-Cheruel *et al.*, Structure-function analysis of pneumococcal DprA protein reveals that dimerization is crucial for loading RecA recombinase onto DNA during transformation. *Proc. Natl. Acad. Sci. U.S.A.* **109**, E2466–2475 (2012).
25. T. Yadav *et al.*, Bacillus subtilis DprA recruits RecA onto single-stranded DNA and mediates annealing of complementary strands coated by SsbB and SsbA. *J. Biol. Chem.* **288**, 22437–22450 (2013).
26. L. Marie *et al.*, Bacterial RadA is a DnaB-type helicase interacting with RecA to promote bidirectional D-loop extension. *Nat. Commun.* **8**, 15638 (2017).
27. R. Torres, E. Serrano, J. C. Alonso, Bacillus subtilis RecA interacts with and loads RadA/Sms to unwind recombination intermediates during natural chromosomal transformation. *Nucleic Acids Res.* **47**, 9198–9215 (2019).
28. T. M. Nero *et al.*, ComM is a hexameric helicase that promotes branch migration during natural transformation in diverse Gram-negative species. *Nucleic Acids Res.* **46**, 6099–6111 (2018).
29. D. Dubnau, M. Blokesch, Mechanisms of DNA uptake by naturally competent bacteria. *Annu. Rev. Genet.* **53**, 217–237 (2019).
30. M. Bergé, I. Mortier-Barrière, B. Martin, J.-P. Claverys, Transformation of Streptococcus pneumoniae relies on DprA- and RecA-dependent protection of incoming DNA single strands. *Mol. Microbiol.* **50**, 527–536 (2003).
31. A. B. Dalia, T. N. Dalia, Spatiotemporal analysis of DNA integration during natural transformation reveals a mode of nongenetic inheritance in bacteria. *Cell* **179**, 1499–1511.e10 (2019).
32. J. Hahn, B. Maier, B. J. Haijema, M. Sheetz, D. Dubnau, Transformation proteins and DNA uptake localize to the cell poles in Bacillus subtilis. *Cell* **122**, 59–71 (2005).
33. D. Kidane, P. L. Graumann, Intracellular protein and DNA dynamics in competent Bacillus subtilis cells. *Cell* **122**, 73–84 (2005).
34. S. Tadesse, P. L. Graumann, DprA/Smf protein localizes at the DNA uptake machinery in competent Bacillus subtilis cells. *BMC Microbiol.* **7**, 105 (2007).
35. J.-P. Claverys, M. Prudhomme, B. Martin, Induction of competence regulons as a general response to stress in gram-positive bacteria. *Annu. Rev. Microbiol.* **60**, 451–475 (2006).
36. T. Lam *et al.*, Competence pili in Streptococcus pneumoniae are highly dynamic structures that retract to promote DNA uptake. *Mol. Microbiol.* **116**, 381–396 (2021).
37. M. J. Bergé *et al.*, Midcell recruitment of the DNA uptake and virulence nuclease, EndA, for pneumococcal transformation. *PLoS Pathog.* **9**, e1003596 (2013).
38. C. H. Johnston *et al.*, The alternative sigma factor σX mediates competence shut-off at the cell pole in Streptococcus pneumoniae. *Elife* **9**, e62907 (2020).
39. C. Johnston, I. Mortier-Barriere, V. Khemici, P. Polard, Fine-tuning cellular levels of DprA ensures transformant fitness in the human pathogen Streptococcus pneumoniae. *Mol. Microbiol.* **109**, 663–675 (2018).
40. E. V. Pestova, L. S. Håvarstein, D. A. Morrison, Regulation of competence for genetic transformation in Streptococcus pneumoniae by an auto-induced peptide pheromone and a two-component regulatory system. *Mol. Microbiol.* **21**, 853–862 (1996).
41. I. Draskovic, D. Dubnau, Biogenesis of a putative channel protein, ComEC, required for DNA uptake: Membrane topology, oligomerization and formation of disulphide bonds. *Mol. Microbiol.* **55**, 881–896 (2005).

42. D. A. Morrison, I. Mortier-Barrière, L. Attaiech, J.-P. Claverys, Identification of the major protein component of the pneumococcal eclipse complex. *J. Bacteriol.* **189**, 6497–6500 (2007).
43. L. Attaiech *et al.*, Role of the single-stranded DNA-binding protein SsbB in pneumococcal transformation: Maintenance of a reservoir for genetic plasticity. *PLoS Genet.* **7**, e1002156 (2011).
44. A. Badrinarayanan, T. B. K. Le, M. T. Laub, Rapid pairing and resegregation of distant homologous loci enables double-strand break repair in bacteria. *J. Cell Biol.* **210**, 385–400 (2015).
45. V. Amarh, M. A. White, D. R. F. Leach, Dynamics of RecA-mediated repair of replication-dependent DNA breaks. *J. Cell Biol.* **217**, 2299–2307 (2018).
46. J. Wiktor *et al.*, RecA finds homologous DNA by reduced dimensionality search. *Nature* **597**, 426–429 (2021).
47. M. Boonstra, N. Vesel, O. P. Kuipers, Fluorescently labeled DNA interacts with competence and recombination proteins and is integrated and expressed following natural transformation of Bacillus subtilis. *mBio* **9**, e01161-18 (2018).
48. R. van Raaphorst, M. Kjos, J.-W. Veening, Chromosome segregation drives division site selection in Streptococcus pneumoniae. *Proc. Natl. Acad. Sci. U.S.A.* **114**, E5959–E5968 (2017).
49. A. M. Oliveira Paiva *et al.*, The bacterial chromatin protein HupA can remodel DNA and associates with the nucleoid in Clostridium difficile. *J. Mol. Biol.* **431**, 653–672 (2019).
50. C. Gallay *et al.*, CcrZ is a pneumococcal spatiotemporal cell cycle regulator that interacts with FtsZ and controls DNA replication by modulating the activity of DnaA. *Nat. Microbiol.* **6**, 1175–1187 (2021).
51. A. S. Dixon *et al.*, NanoLuc complementation reporter optimized for accurate measurement of protein interactions in cells. *ACS Chem. Biol.* **11**, 400–408 (2016).
52. I. Mortier-Barrière, P. Polard, N. Campo, Direct visualization of horizontal gene transfer by transformation in live pneumococcal cells using microfluidics. *Genes* **11**, E675 (2020).
53. N. C. Brown, 6-(p-hydroxyphenylazo)-uracil: A selective inhibitor of host DNA replication in phage-infected Bacillus subtilis. *Proc. Natl. Acad. Sci. U.S.A.* **67**, 1454–1461 (1970).
54. V. Khemici, M. Prudhomme, P. Polard, Tight interplay between replication stress and competence induction in Streptococcus pneumoniae. *Cells* **10**, 1938 (2021).
55. J. D. Wang, G. M. Sanders, A. D. Grossman, Nutritional control of elongation of DNA replication by (p) ppGpp. *Cell* **128**, 865–875 (2007).
56. C. Johnston *et al.*, RecFOR is not required for pneumococcal transformation but together with XerS for resolution of chromosome dimers frequently formed in the process. *PLoS Genet.* **11**, e1004934 (2015).
57. J. Hahn, A. W. Tanner, V. J. Carabetta, I. M. Cristea, D. Dubnau, ComGA-RelA interaction and persistence in the Bacillus subtilis K-state. *Mol. Microbiol.* **97**, 454–471 (2015).
58. M. Prudhomme, L. Attaiech, G. Sanchez, B. Martin, J.-P. Claverys, Antibiotic stress induces genetic transformability in the human pathogen Streptococcus pneumoniae. *Science* **313**, 89–92 (2006).
59. J. Slager, M. Kjos, L. Attaiech, J.-W. Veening, Antibiotic-induced replication stress triggers bacterial competence by increasing gene dosage near the origin. *Cell* **157**, 395–406 (2014).
60. C. Johnston, N. Campo, M. J. Bergé, P. Polard, J.-P. Claverys, Streptococcus pneumoniae, le transformiste. *Trends Microbiol.* **22**, 113–119 (2014).
61. F. Lecointe *et al.*, Anticipating chromosomal replication fork arrest: SSB targets repair DNA helicases to active forks. *EMBO J.* **26**, 4239–4251 (2007).
62. A. Costes, F. Lecointe, S. McGovern, S. Quevillon-Cheruel, P. Polard, The C-terminal domain of the bacterial SSB protein acts as a DNA maintenance hub at active chromosome replication forks. *PLoS Genet.* **6**, e1001238 (2010).
63. R. D. Shereda, A. G. Kozlov, T. M. Lohman, M. M. Cox, J. L. Keck, SSB as an organizer/mobilizer of genome maintenance complexes. *Crit Rev. Biochem. Mol. Biol.* **43**, 289–318 (2008).
64. B. Martin, M. Prudhomme, G. Alloing, C. Granadel, J. P. Claverys, Cross-regulation of competence pheromone production and export in the early control of transformation in Streptococcus pneumoniae. *Mol. Microbiol.* **38**, 867–878 (2000).
65. A. Dagkessamanskaia *et al.*, Interconnection of competence, stress and CiaR regulons in Streptococcus pneumoniae: Competence triggers stationary phase autolysis of ciaR mutant cells. *Mol. Microbiol.* **51**, 1071–1086 (2004).
66. M. J. Bergé *et al.*, A programmed cell division delay preserves genome integrity during natural genetic transformation in Streptococcus pneumoniae. *Nat. Commun.* **8**, 1621 (2017).
67. A. Ducret, E. M. Quardokus, Y. V. Brun, MicrobeJ, a tool for high throughput bacterial cell detection and quantitative analysis. *Nat. Microbiol.* **1**, 16077 (2016).
68. K. J. Livak, T. D. Schmittgen, Analysis of relative gene expression data using real-time quantitative PCR and the 2(-Delta Delta C(T)) Method. *Methods* **25**, 402–408 (2001).